Available online at www.sciencedirect.com

jmr&t Journal of Materials Research and Technology

journal homepage: www.elsevier.com/locate/jmrt

Original Article

Impact of surface texture on ultrasonic wire bonding process

Yangyang Long [a,*], Matthias Arndt [b], Folke Dencker [b], Marc Wurz [b], Jens Twiefel [a], Jörg Wallaschek [a]

[a] Institute of Dynamics and Vibration Research, Leibniz Universität Hannover, An der Universität 1, 30823 Garbsen, Germany

[b] Institute of Micro Production Technologies, Leibniz Universität Hannover, An der Universität 2, 30823 Garbsen, Germany

ARTICLE INFO

Article history:
Received 17 June 2022
Accepted 24 July 2022
Available online 10 August 2022

Keywords:
Ultrasonic wire bonding
Surface texture
Oxide removal
Microweld formation
Bonding mechanisms
Process window

ABSTRACT

Due to the complex mechanisms, the ultrasonic (US) wire bonding process is usually optimized in the way of varying the processing parameters including normal force, US power, and processing time. In this study, a new way by creating different surface textures on substrates was used to alter the bonding process and improvements of the bonding process were detected. Three different surface textures including deposited strips, straight ditches at different angles, and elliptic ditches were designed and created on glass substrates. The results showed that the elliptic ditches hardly influence the bonding process while the deposited strips and straight ditches significantly alter the bonding process. The deposited strips help break the oxide scale and facilitate the transportation of oxides to the outside of contact. With the straight ditches, the oxide removal efficiency was significantly enhanced. Especially when the driving current exceeded 0.45 A, long chips from the ditches were clearly observed during the bonding process. The chips were aluminum and aluminum oxide which were continuously cut from the wire, accumulated in the ditches, pressed and squeezed to the outside of the contact. With a different angle of the straight ditches, the shape of the bonding footprint can be changed correspondingly. Compared to the bonding on smooth surfaces, the bonding strength on substrates with deposited strips and straight ditches was a few times higher and had a smaller deviation. The bonding process window was significantly enlarged.

1. Introduction

Ultrasonic (US) wire bonding has been widely applied in electronic packaging for more than half a century [1]. Due to the complexity of the process, the underlying mechanisms are still not completely understood. As a result, there is only one way to change the process, i.e., varying the processing parameters including normal force, US power and processing time. In industry and most research work, design of

* Corresponding author.
E-mail addresses: long@ids.uni-hannover.de, lyysdll@gmail.com (Y. Long).

https://doi.org/10.1016/j.jmrt.2022.07.187

experiments is used to optimize these parameters so that the bonding strength can be maximized. If a further enhancement of the joining strength is desired, an alternative way to change the bonding process shall be found. To achieve this, the state-of-the-art understanding of the mechanisms has to be surveyed.

The wire bonding process is typically finished in a few tens to a few hundreds of milliseconds by applying normal force and US vibration. In general, the bonding process contains four phases [2,3] (the ball bonding has an additional electronic flame-off phase in the beginning): (1) Pre-deformation and activation of vibration, (2) Friction, (3) Ultrasonic softening, and (4) Interdiffusion and recrystallization. The pre-deformation of the wire is caused by the loading of normal force (touchdown force), leads to the crack of the oxide scale, and creates an elliptic contact between wire and substrate. After a short period of activation of vibration, the second phase – friction – begins. The relative motion between the wire and the substrate detaches the oxide flakes from the pure metal surface, mills the flakes into small particles, and transports the particles to the peripheral contact area or the outside of the contact area [4,5]. The transportation is accomplished by penetration, oxide flow, metal splash and pushing [4]. Until oxides are removed, microwelds cannot be formed in the corresponding location. Therefore, the main function of the friction phase, oxide removal, is essential to the bonding process. The softening effect leads to the expansion of the contact area at mesoscale [6], and the formation of direct metal–metal contact (i.e., microweld) at atomic-scale [7]. Interdiffusion between the wire and substrate materials takes place after the formation of microwelds [8]. The dynamic stress caused by vibration also leads to the recrystallization of the joining partners, especially at the interface [9]. Depending on the strength of local microwelds and the vibration-induced horizontal stress, the already-formed microwelds can be broken and re-formed. The competition between the formation and breakage of microwelds determines the final bonding strength [10].

The above-mentioned mechanisms are changed when the processing parameters are varied. A large normal force inhibits the relative motion between wire and substrate, which adversely influences the removal of oxides, and thus less microwelds can be formed. When the normal force is small, the vibration-induced horizontal stress can be large enough to break large portions of microwelds. As for US power, a high power can be detrimental to the already-formed microwelds while a low power is not sufficient to remove oxides. A short processing time is not long enough for the growth of microwelds and a long processing time can also be harmful for the joining. Therefore, a processing window needs to be found and applied. Besides finding the processing window, the geometry of the bonding tool was explored in order to reduce the tool wear for copper wire bonding. Different geometries, including decreasing the groove height [11], enlarging the groove angle [12], and adding three ridges [12], were tested. A significant wear reduction was detected and the lifetime of the tool was significantly elongated. However, the influence on the bonding process at the wire/substrate interface was insignificant.

The survey shows that a possible way to alter the bonding process is to create surface textures on either the wire or on the substrate. For the purpose of research and demonstration, it is easier and more economic to operate on the substrate surface. Thus, in this work, different surface textures were designed and tested. In the following sections, the design and manufacturing of the textures are first illustrated. The results with corresponding textures are then described in detail.

2. Experiments

2.1. *Design of surface textures*

To study the influence of surface texture on the bonding process, different textures were designed. In order to observe the bonding process occurring at the wire/substrate interface, glass substrates were used in this study. As shown in Fig. 1 (a), titanium strips with different widths (5 μm and 10 μm) were deposited on a 3 mm glass substrate with different interval distances (50 μm and 100 μm). The deposition thickness was set as 200 nm which is close to the surface roughness of the wire. The design of such a strip texture has two purposes. First, the edges of the strips were supposed to help break the oxide scale of the wire. Second, oxide particles

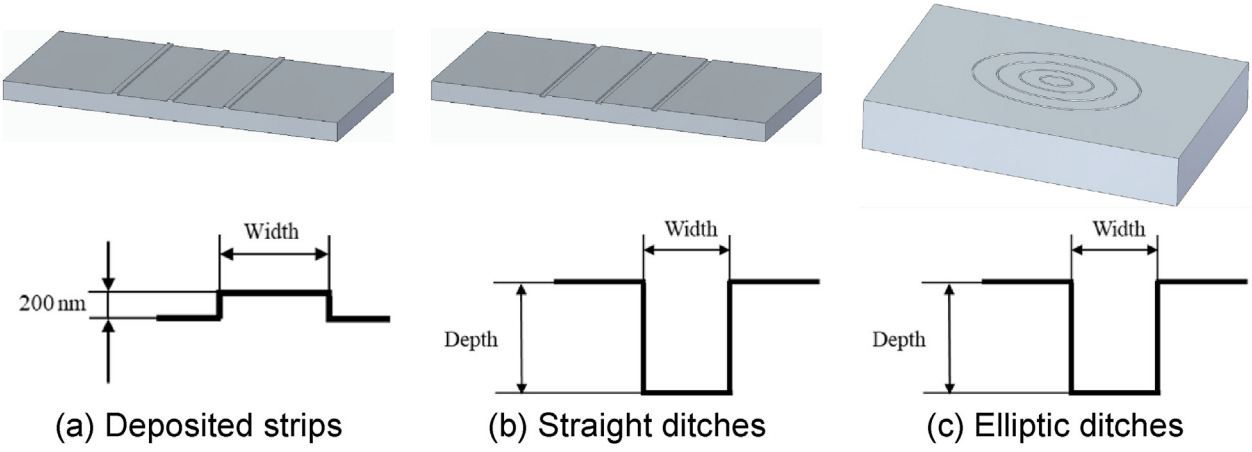

Fig. 1 – Illustration of three different surface textures for wire bonding.

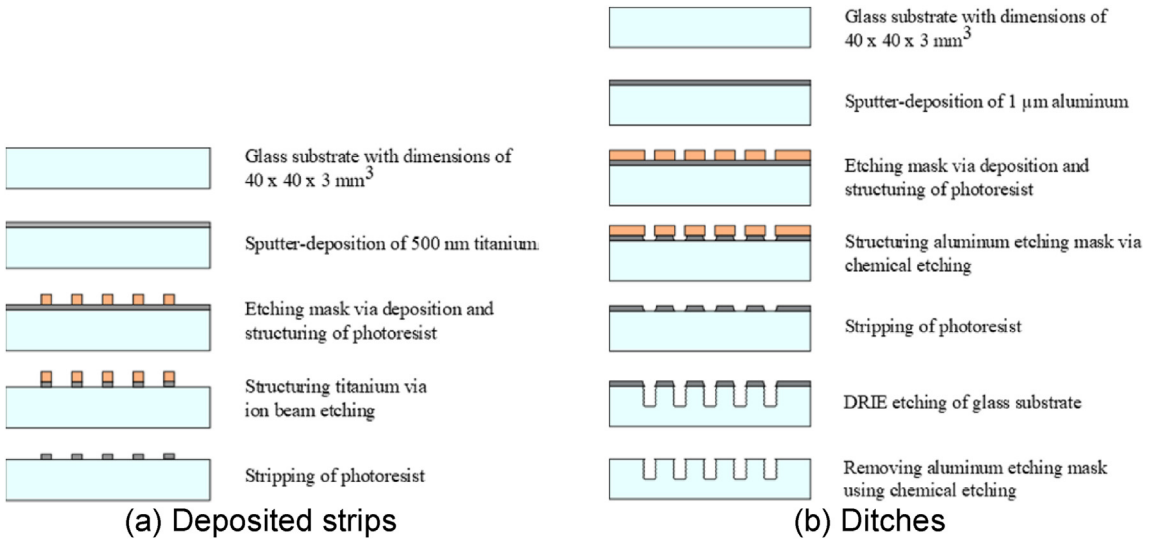

Fig. 2 – Manufacturing process of the surface texture on glass substrate.

were assumed to be more easily transported along the strips to the outside.

Straight ditches with different widths (10 μm and 20 μm) and depths (2 μm and 5 μm) were etched on glass substrates, as shown in Fig. 1 (b). The interval distance between ditches varied between 50 μm and 200 μm. The edges of the ditches were also supposed to help break the oxide scale. The ditches were assumed to transport and store oxides. The angle between the ditches and the wire direction varied at 0°, 45° and 90°. Beside straight ditches, elliptic ditches corresponding to the shape of wire bonding footprint were also designed as in Fig. 1 (c). The main purpose of this design was to provide storage space for oxide particles on the expansion path of the contact area.

2.2. *Manufacturing of surface textures*

Microproduction of the desired textures within the glass (40 x 40 × 3 mm^3) has been achieved in a combination of lithography and etching processes. In this context, two different approaches have been applied for producing either titanium strips on top of the glass surface or ditches directly within the glass.

For the deposited strips as in Fig. 1 (a), the desired layout was transferred with the help of photolithography (Fig. 2 (a)). First, titanium was sputter-deposited on top of the entire glass area. A negative photoresist was then used to create a temporary etching mask with the shape of the lines, respectively. Finally, the titanium layer in the unprotected parts was removed via ion beam etching (IBE) and the photoresist was stripped off.

For the second approach, the structures as in Fig. 1 (b) (c) were patterned on the glass substrate via deep reactive ion etching (DRIE). Trenches with steep sidewalls can thus be accomplished. To limit the etching to the intended areas, an etching mask made of aluminum was used, which provided sufficient selectivity in the following DRIE process. Therefore, a 1 μm thick aluminum layer was sputter deposited on top of the glass surface first. Producing the right pattern in the aluminum was then accomplished with the aid of a structured photoresist mask and a wet chemical etching process using peroxymonosulfuric acid as etching solution. After removing the photoresist, the substrate was ready for the DRIE process.

DRIE was run on the ICP-based Plasmalab System 100 by Oxford Instruments. The process consisted of two repeatedly executed modes to achieve an etch depth of 2 or 5 μm with nearly vertical sidewalls. In the first mode, an isotropic plasma etch attack of the glass substrate took place with the help of C_4F_8 and O_2. At the same time, argon ions were accelerated by an overlayed electrical field towards the glass, creating an additional physical and anisotropic material removal. This physical etching helped eliminate the chemically inert passivation layer of C_4F_8, which was deposited onto the substrate's surface in the second mode to prevent further chemical etching. Since the ions removed the passivation layer at the bottom of the trench much faster than along the sides, the chemical etching took only place at the bottom. Hence, the entire process became anisotropic as well. After the pattern of the aluminum layer had been transferred to the glass substrate, the aluminum was finally removed with the help of peroxymonosulfuric acid.

2.3. *Wire bonding*

A thick wire bonding head HBK05 from Hesse Mechatronics GmbH was used to perform US wire bonding. The US transducer of the bonding head has a natural frequency of ~60 kHz and was controlled by an in-house made controller PLL500/100 k. The bonding wire was Al–H11 aluminum wire (diameter 400 μm) from Heraeus GmbH. From our preliminary study, 5 N normal force is the optimal force for 400 μm Al-glass bonding. Thus, only 5 N was applied in this work while the driving current which corresponds to the vibration amplitude (1 A corresponds to 5 μm) varied.

2.4. *Optic observation and SEM measurements*

A real-time observation system was placed beneath the bonding site to record the bonding process as in Fig. 3. It has a resolution of 1.1 μm/pixel and a frame rate of 20,000 f/s was used in this work. Illumination was provided by a high-performance Xenon cold light source. Details of the setup were described in [6]. The bonding interface after shear test and the element distribution were measured by a Zeiss LEO 1455 V P Scanning Electron Microscope equipped with an Oxford Energy Dispersive Spectroscopy (EDX).

3. Results and discussions

In this section, the bonding processes on deposited strips, straight ditches, and elliptic ditches are described based on the real-time observation. The underlying mechanisms and their differences from those of smooth surface bonding [5] are then discussed. The influence of the textures are finally evaluated by shear tests and SEM measurements.

3.1. *Deposited strips*

A typical bonding process on the deposited strips was recorded and provided in Supplemented Material 1 (S1). Representative images were subtracted from the video and are shown in Fig. 4. The width and height of the strips were 5 μm and 200 nm respectively. The strips were perpendicular to the wire direction and the interval distance between strips was 50 μm. As shown in Fig. 4 (a), an elliptic contact, as marked by the blue curves, was formed at the bonding interface after normal force loading. A bright line also showed up on the left side of each strip. As vibration started, the bright lines became thinner when the wire vibrated to the right, and became thicker when the wire vibrated to the left. This phenomenon can be clearly observed in the Video S1. In the meantime, the contact area expanded due to softening effect. After about 5 ms, the oxide flakes started to be milled into small particles and the corresponding areas became bright. The image in Fig. 4 (b) showed that the milling first took place at inner peripheral region where the friction energy was the highest as stated in [13]. The bright area covered the inner area in about 14 ms and covered the outer peripheral area in about 22 ms. It was not clear in the video whether oxide particles flew along the strips to the outside or not. Nevertheless, the inner area became darker again from 25.5 ms which indicates the transportation of oxide particles from this area to the surrounding area. In addition, the moving of a large number of oxide particles to the outside of the contact can be observed at the contact boundary, as marked by the red circles in Fig. 4 (c). From about 116 ms, static dark area, indicating the formation of microwelds, appeared. Obvious particle flow from the right side to the left can be observed after about 161 ms. The flow situation at 186 ms was marked by the arrows in Fig. 4 (d). Due to the vibration induced friction reduction, particles would flow from high normal stress areas to low normal stress areas. Thus, these arrows also indicted the normal stress distribution with the strips. The microweld area at 293.1 ms is marked in the red border of Fig. 4 (e) while the area marked by the purple circle shows large amounts of oxide particles. From this moment until about 318 ms, a fast growth of microweld area was observed. After this period, the growth of microweld area nearly stopped. On the other hand, large amounts of particles finally remained in the static area (see the marked area of Fig. 4 (f)), which indicated a low oxide removal efficiency. This is in conflict with the conclusion based on the observation in the first ~100 ms. Therefore, from the video alone, it is hard to judge whether the oxide removal efficiency was enhanced or not.

Supplementary video to this article can be found online at https://doi.org/10.1016/j.jmrt.2022.07.187.

The strips made the process different from that on smooth surface, so as the underlying mechanisms. As for bonding on smooth surface, no bright lines were observed after the normal force loading, unless an additional oxide layer was coated [4]. The bright lines here on the left of strips indicate that the oxide scale or even the wire material at the edges had cracked due to concentrated stresses. Compared to flat surfaces, the crack surfaces could reflect more light into the camera. Such bright lines should appear on the other side of

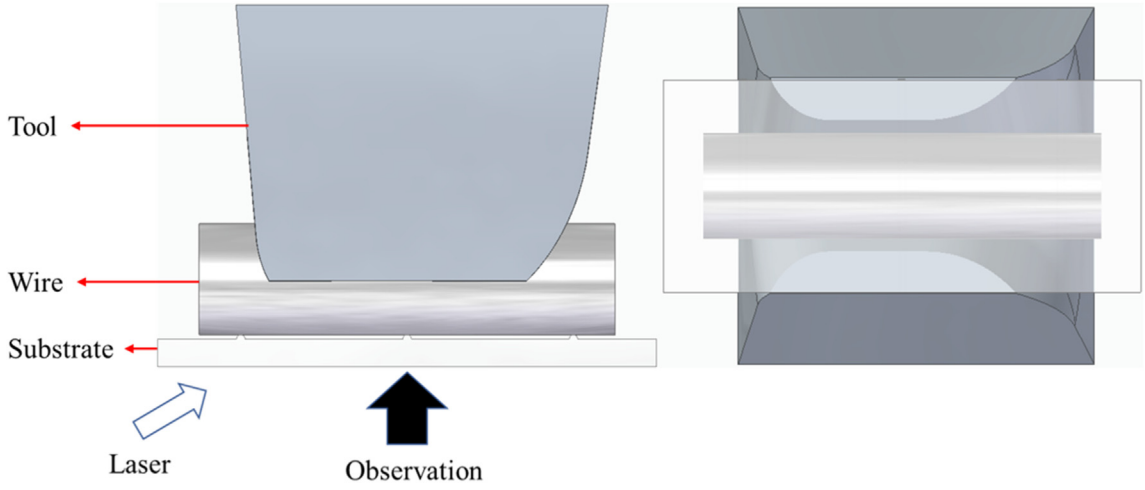

Fig. 3 – Direct observation of the bonding interface from bottom.

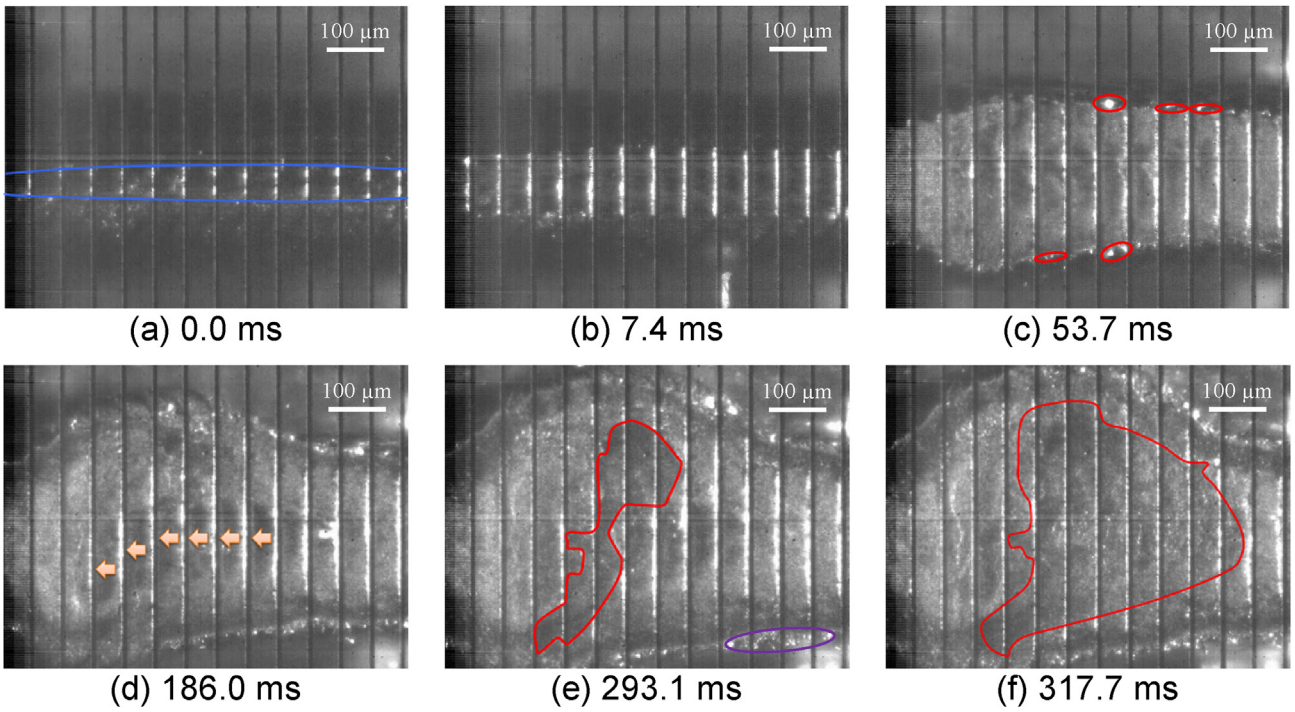

Fig. 4 – Wire bonding process with deposited Ti strips under 5 N, 0.50 A.

the strips as well. However, since the illumination light was provided from the right side, the crack surfaces on the right side, which faced the left side, could not be observed. The width changes of the bright lines, which did not occur for bonding on smooth surfaces, were due to the compression and tension of the cracks as the wire vibrated forth and back. The milling of the oxide flakes first take place in the inner peripheral region, and then expanded to both the inner region and outer peripheral region, which followed the same order as that on smooth surfaces. The change of the color (bright to dark in the inner area) occurred at an early time and a larger number of particles moved to the outside, compared to those on smooth surface. All these imply a more efficient oxide transportation process with the strips, which will be later validated by the shear tests. After the removal of oxides, microwelds can be formed in those clean areas. The above described microweld growth, from a small inner area to finally a large area, was similar to that on smooth surface and no significant difference was observed. In general, the cracking, and transportation of oxides were significantly altered by the deposited strips.

Another point needs to be noted here is the material of the strips – titanium, which is a well-known bonding material. Different from the ditches, joining can occur on the titanium

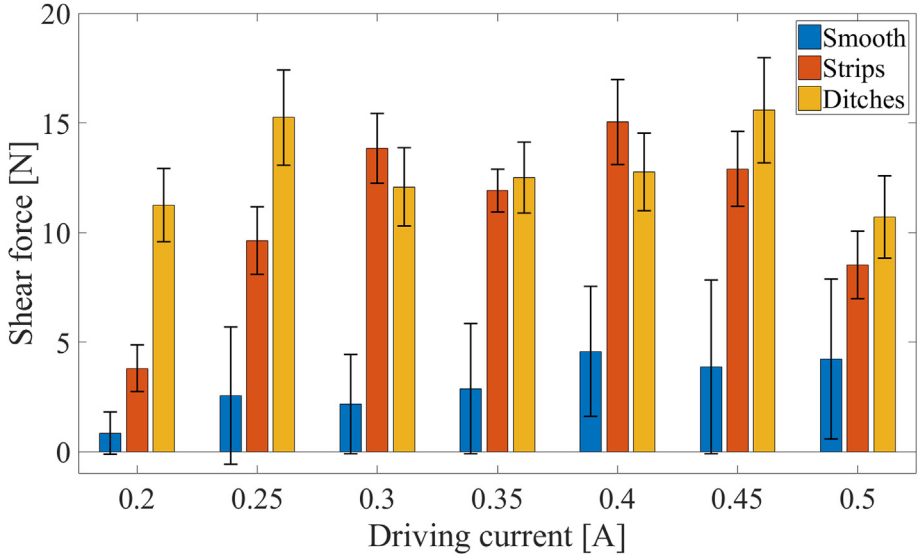

Fig. 5 – Shear strength of bonding on smooth, strip and ditch surfaces under 5 N normal force and different driving currents.

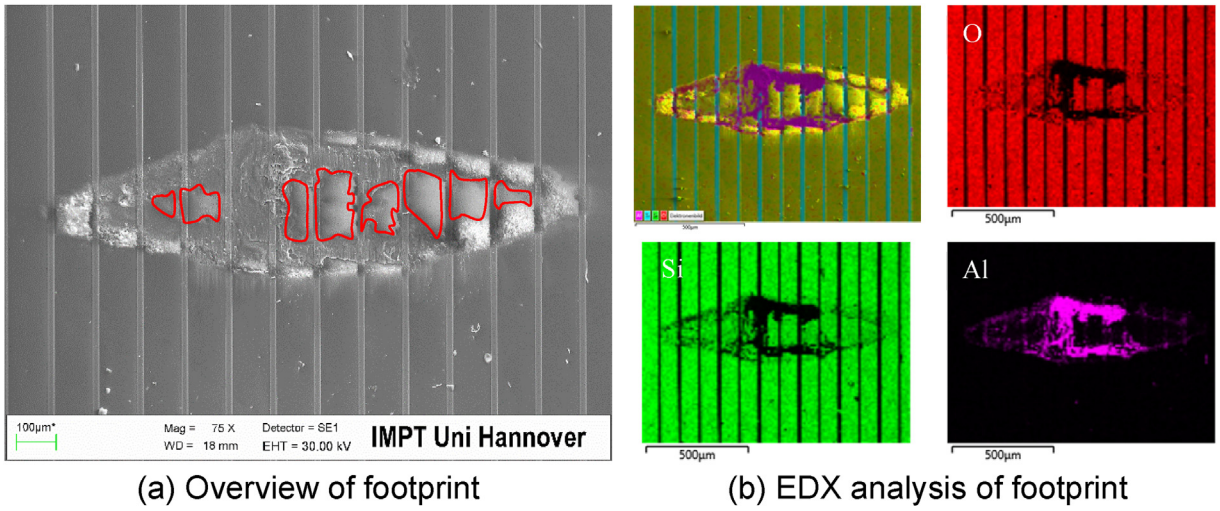

Fig. 6 – SEM/EDX measurements of a bonding on strips of 20 μm width, 200 nm height and 100 μm interval distance under 5 N, 0.4 A.

made strips. Once microwelds are formed between the aluminum wire and the titanium strips, interdiffusion occurs at a much higher rate under the effect of US vibration and IMC will be formed. Typically, the strength of the joining (IMC region) is higher than that of pure aluminum. This is also true to the Al-glass bonding: the strength of the joining region is higher than that of pure aluminum even though there is no IMC formation. That is to say the shear strengths measured by shear tests show no significant difference between Al–Ti and Al-glass bonding when the joining areas are the same, since the breakage of material due to shearing takes place on pure aluminum, not at the interface. From this point of view, the contribution of titanium to the bonding strength is insignificant, compared to the bonding on smooth glass surface.

To further test if the oxide removal efficiency was enhanced by the deposited strips, shear tests and SEM/EDX measurements were conducted. The result of shear tests is shown in Fig. 5. It can be seen that the shear strength of bonds on the strip texture is much higher than that on smooth surfaces. In addition, the standard deviation as indicated by the error bar is smaller as well. This means that the total microweld area formed on the strip texture was large. The prerequisite to a large microweld area was that the oxides were removed in that area. Thus, the shear tests indicated a higher oxide removal efficiency with the deposited strips. Fig. 6 shows the footprint of a bond on the strip texture and the corresponding element distribution. Microwelds can be clearly observed in part of the inner peripheral region and part of the inner area, as indicated by the purple color in Fig. 6 (b). The bright area in the peripheral region in Fig. 6 (a) shows that substantial wear was caused during the bonding process and the glass surface was seriously damaged. Many aluminum oxides can also be found in this region. Another interesting and unique feature is the delamination of glass, as marked by the red borders in Fig. 6 (a). No microweld and no particles can be found in these areas. This feature has been observed in all specimens with the strip texture while it is not clear why this happened. Together with the shear test result, it is deduced that the oxide removal efficiency was significantly enhanced.

Similar processes happened when strips with different widths and different interval distances were used, but only when the strips were perpendicular to the wire direction. When the strips were parallel to the wire direction, no clear differences from the bonding on smooth surfaces were observed. In general, compared to the bonding on smooth surfaces, the cracking of oxide scale directly occurred after the normal force loading; the transportation of oxide particles occurred at an early time and more oxides can be removed from the contact region. As a result, a higher bonding strength was achieved.

3.2. *Straight ditches*

The bonding process became very different with straight ditch texture, especially when the ditches were perpendicular to the wire direction. Such a process was recorded and can be found in Supplemented Material 2 (S2). Fig. 7 shows some representative images of the video. The ditches have a width of 20 μm and a depth of 5 μm, and the interval distance between ditches is 200 μm. Different from the bonding on deposited strips, the whole ditch area instead of just the right side showed a high brightness after the normal force loading. As the wire started to vibrate back and forth, the widths of the bright lines changed as in S2. After about 2 ms, clear particle shapes could be observed along the bright lines. From then on, the bright lines had irregular shapes due to the different distributions of particles. Such a distribution at 21 ms is shown in Fig. 7 (a). After about 24 ms, more bright areas showed up on the smooth surfaces between ditches. The oxide flakes in these areas had been milled into particles. These new bright areas started at the two sides of the ditches and expanded to the middle of the smooth surfaces, see from Fig. 7 (a)–(b). Attention needs to be paid to the marked area in Fig. 7 (b) where a chip started to be generated from the ditch. As the process continued, the chip was continuously squeezed out from the ditch and grew longer. As marked in the red circle of Fig. 7 (c), the chip had grown to around 100 μm in 5 ms. More chips were generated during this period. The chip in the blue

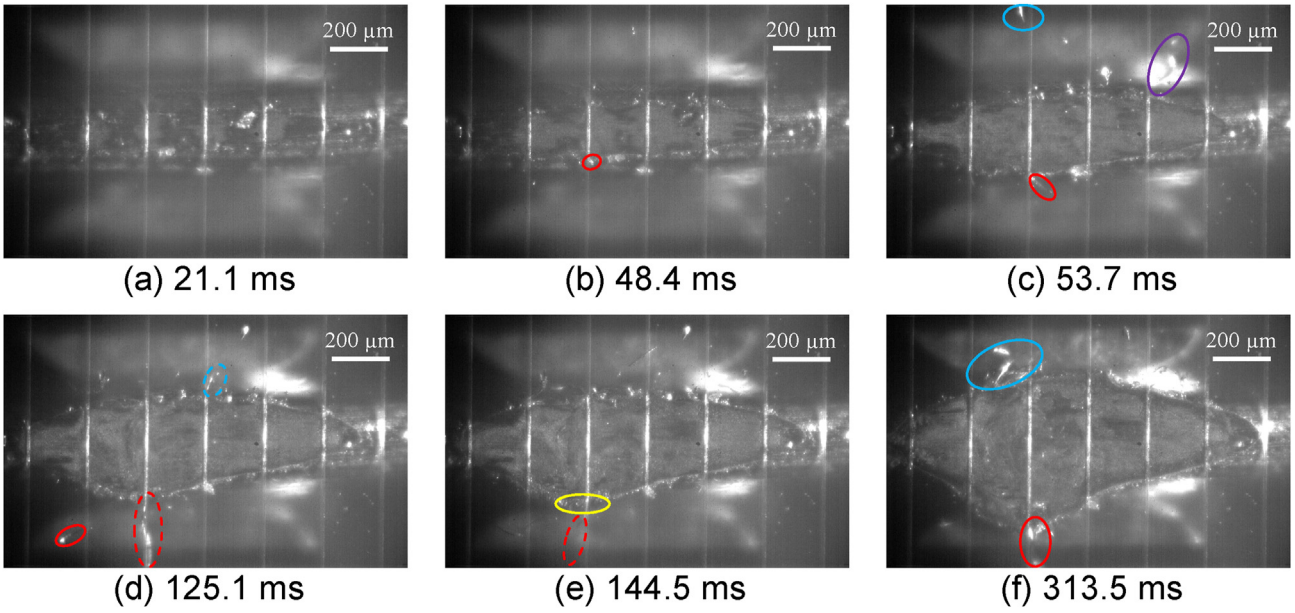

Fig. 7 – Wire bonding process with straight ditches of 20 μm width, 5 μm depth and 200 μm interval distance under 5 N, 0.5 A.

circle had been "cut off" from the 4th ditch (from left) while the chip in the purple circle kept growing from another ditch (the 5th from left). The length of the chip in the purple circle was around 250 μm, which was much longer than the contact length (about 200 μm) on the 5th ditch. The generation of chips did not stop when a chip was broken, such as the one in the blue circle of Fig. 7 (c). As marked in the blue dash circle of Fig. 7 (d), a new chip was generated from the position where the old chip was "cut". The same thing occurred on the 3rd ditch. The old chip marked in the red circle of Fig. 7 (c) was cut at the lower boundary of the 3rd ditch and jumped to the position marked in the red circle of Fig. 7 (d). A new chip was then generated and had grown to a much longer one as marked in the red dash circle of Fig. 7 (d). The generation of chips also facilitated the generation of metal splashes. The red dash circle in Fig. 7 (e) marked a new chip. Along the growing of this chip, a metal splash, as marked in the yellow circle, was generated and kept growing as well. After about 190 ms, the chip at the splash position stopped growing, became part of or attached to the splash, and moved to the outside of the ditch, which is similar to the red marked area in Fig. 7 (f). The blue marked area in Fig. 7 (f) shows many chips, which were transported to the outside.

The high brightness over the whole ditch area implies that many cracks or even some particles had been generated in the ditch area due to the edge cutting of ditches and the local deformation of wire. The changes of the bright line width and the particle distribution in the ditches were caused by the compression and tension of local wire as well as the relative motion between local wire and ditch surfaces. The ditches did change the order of the milling process. Unlike the milling on strip texture or on smooth surfaces, the milling on the ditch texture first occurred on the border of ditches and then expanded to the middle of the smooth surface area. The most significant difference is the generation of chips, which had never been observed before. The continuous generation and the larger length over the contact length at the ditches indicate that a chip was not a single part of material directly cut from the wire. Instead, a number of small volume of materials, including both aluminum and aluminum oxide, were continuously cut from the wire and stored in the ditches. These stored materials were pressed and then squeezed out to form chips. This assumption was validated by SEM/EDX measurements which will be described later. By sacrificing a small volume of wire material (pure aluminum), large amounts of oxides were carried to the outside. By facilitating the generation of metal splashes, the oxide removal efficiency was further promoted [4]. In summary, the ditch texture significantly changed the cracking, milling and transportation of oxides.

The chip generation was very often observed on the straight ditch texture when the driving current exceeded 0.45 A. This is independent of the width, the depth and the interval distance of the ditches. Another two examples are shown in Fig. 8. Fig. 8 (a) shows a bonding on a ditch texture with a smaller interval distance. At the moment, the growing of two chips can be observed as marked in the red and blue circles. Metal splashes also occurred later at these two positions. Fig. 8 (b) shows a bonding on a shallow (2 μm deep) ditch texture. The generated chips were also marked. For the chips in the yellow circle, the left chip was first generated. After this chip became part of the metal splash and moved to the outside of the corresponding ditch, the right chip appeared and started to grow. When the driving current was below 0.45 A, only short chips or debris were observed while long chips rarely showed up. Nevertheless, an efficient oxide removal process was still achieved.

Compared with bonding on smooth surfaces, more oxides can be removed with the ditch texture and thus the total microweld area became larger. As shown in Fig. 5, the bonding

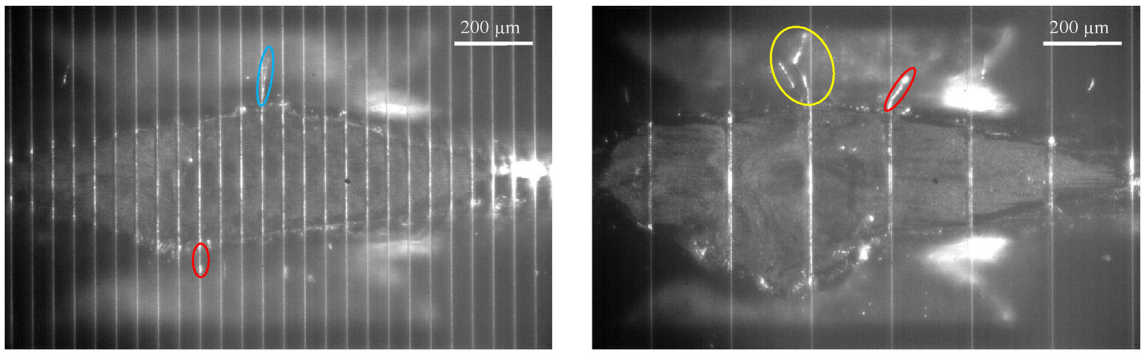

(a) 78.5 ms during bonding on ditches of 10 µm width, 5 µm depth and 50 µm interval distance under 5 N, 0.45 A

(b) 181.6 ms during bonding on ditches of 20 µm width, 2 µm depth and 200 µm interval distance under 5 N, 0.54 A

Fig. 8 – Chip generation during wire bonding under different ditch configurations.

strength was a few times higher and the deviation of the bonding strength was smaller. In addition, the texture significantly enlarged the bonding process window. A high bonding strength can be obtained over the driving current range from 0.2 A to 0.5 A. To reach a similar bonding strength on smooth surfaces, a specific driving current profile like Fig. 9 had to be applied and typical current value in the last constant stage was between 0.25 A and 0.35 A. The high driving current in the first ~200 ms was for efficient removal of oxides and the low driving current in the last ~150 ms was to avoid the damage of already-formed microwelds. Comparably, the bonding process window with smooth surfaces was very small and the control became much harder.

A bonding on ditches of 10 µm width, 5 µm depth and 50 µm interval distance under 5 N, 0.45 A was analyzed by SEM/EDX after the shear test and the results are shown in Fig. 10. The overview of the footprint in Fig. 10 (a) exhibited large areas of aluminum residuals. In addition, part of the glass surface was delaminated during the shear test. These indicate a very strong bond and is in agreement with the shear test (19.5 N). Large amounts of particles can be found in the peripheral contact region. A close observation on the peripheral region shows substantial wear as in Fig. 10 (b), which was caused by the vibration-induced friction. Three types of particles were observed: spherical particles, rod-like particles (high ratio of length over diameter) and irregular particles. Spherical particles stayed mainly inside the contact while rod-like particles were directly located on the outside of the contact border. Irregular particles can be found everywhere. Spherical particles were assumed to originate from the inside contact area and were transported to the peripheral region. During the transportation, the particles rolled like snowballs and thus formed a spherical shape. The rod-like particles were mainly formed at the contact boundary and were pushed away during the expansion of the contact. Irregular particles were also formed during the transportation. In fact, spherical particles were just a special case of the irregular particles which consisted of many smaller particles [5]. Some of the irregular particles were also transported to the outside of the contact. Fig. 10 (d) shows particles which were transported to the outside of the contact. The EDX mapping in Fig. 10 (e) shows that these particles were mainly made from aluminum. Naturally, the surfaces of these aluminum particles were covered by aluminum oxide with an average thickness of 5 nm

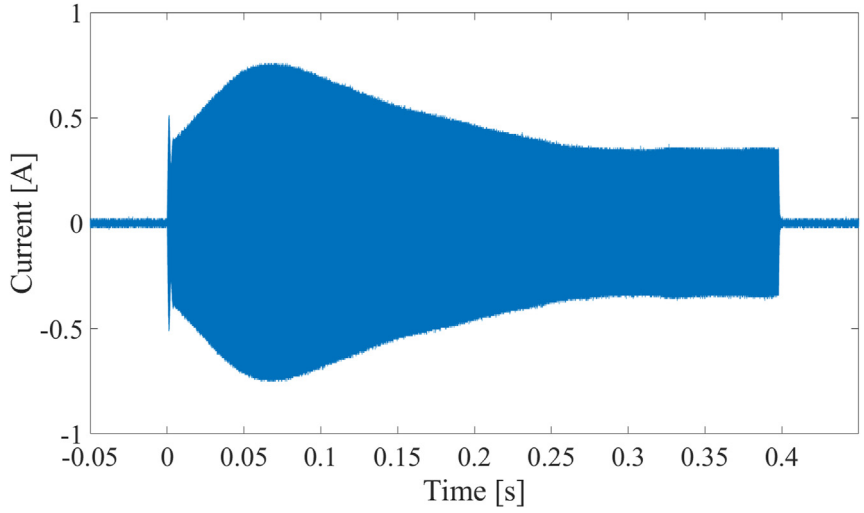

Fig. 9 – Driving current profile for high bonding strength with smooth glass.

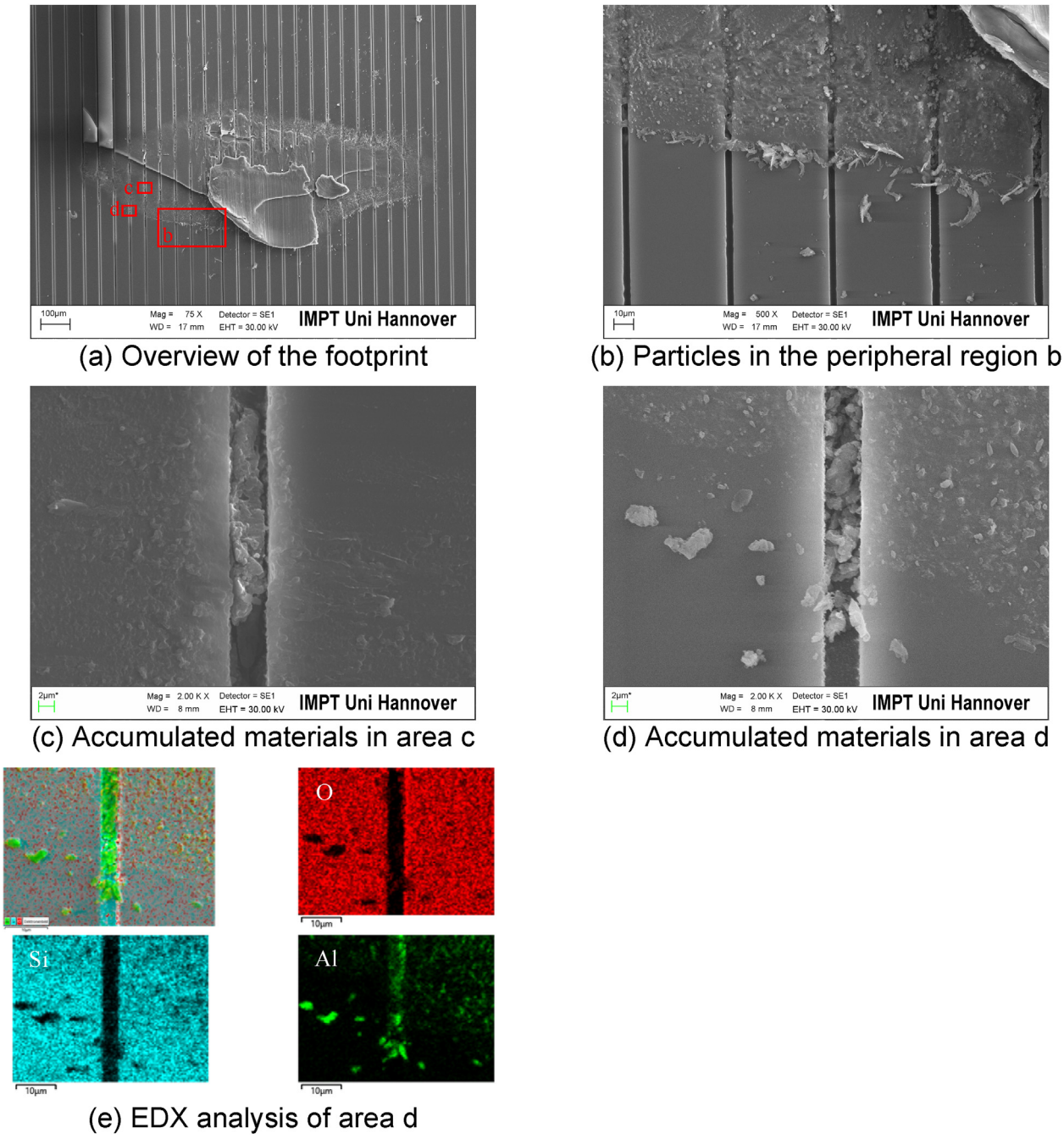

Fig. 10 – SEM/EDX measurements of a bonding on ditches of 10 μm width, 5 μm depth and 50 μm interval distance under 5 N, 0.45 A.

which is hard to be detected by EDX. When the aluminum was cut from the wire, oxides attached to these aluminum materials also fell down into the ditches. A similar area within the contact is shown in Fig. 10 (c). The material inside the ditch was also measured as aluminum by EDX. Differently, the particles were pressed and squeezed into a single part with a layered structure. The chips, which had been transported to the outside of contact, also have a layered structure. These observations validated the previous assumption that some wire materials were cut into the ditches, pressed and squeezed into long chips, and finally transported to the outside.

Ditches were also created at 45° with respect to the wire direction. A typical bonding process on such a 45° ditch texture is provided in Supplemented Material 3 (S3). A few representative images were subtracted and are shown in Fig. 11. As can be seen from the figure, chips as well as metal splashes were still generated. Different from the bonding on perpendicular ditches, the contact line with the ditches did not show a high brightness after the normal force loading. As

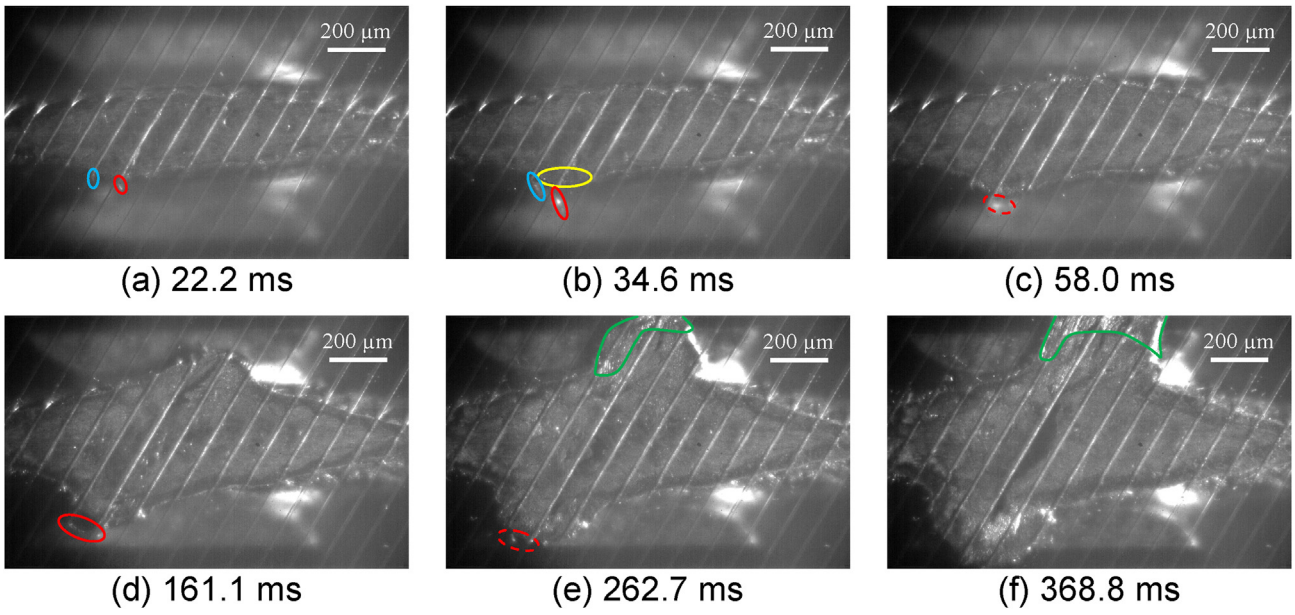

Fig. 11 – Wire bonding process with 45° ditches of 20 μm width, 5 μm depth and 100 μm interval distance under 5 N, 0.70 A.

vibration started, bright areas appeared at the middle (in the ditch direction) of the ditches. The bright areas then expanded to the surrounding areas. From about 17 ms, chips started to be generated. At 22.2 ms, these chips can be observed as the marked areas in Fig. 11 (a). The chips then kept growing while they bent up during the growth. At the moment of Fig. 11 (b), they had grown to more than 100 μm in length. Accompanying with the chips, a metal splash was generated in the same area as marked in the yellow circle of Fig. 11 (b). As the process continued, the chip in the red circle of Fig. 11 (b) was detached and a new chip was generated as in the red dash circle of Fig. 11 (c). From Fig. 11 (c)–(d), an obvious contact expansion in the ditch direction was observed. This indicates that the ditches made the material flow during contact expansion easier. During this period, a new chip was formed and grew as marked in the red circle of Fig. 11 (d). The contact area continued to expand along the ditch direction as observed in Fig. 11 (e), (f). In addition, substantial metal splash was generated as marked by the green curves. The red dash circle in Fig. 11 (e) marked another new chip. Through the whole process, a chip with a total length of about 700 μm was generated from the single ditch, which implies a high efficiency of material removal.

Wire bonding was also performed on ditches in parallel to the wire direction. No substantial difference from the bonding on smooth surfaces was found.

3.3. *Elliptic ditches*

The bonding on elliptic ditches was similar to that on smooth surfaces. The few differences are shown in Fig. 12. As shown in Fig. 12 (a), the milling of oxide flakes started not only in the peripheral contact region, but also in the center ditch. The ditches therefore helped the milling of flakes into particles. At the moment of Fig. 12 (b), the bright area had covered the whole contact area and kept growing. From about 108 ms, static area appeared. The static area at 289 ms was marked in the purple border of Fig. 12 (c). Inside the static area, many bright areas can still be observed which means lots of oxide particles remained inside the static area. The shear tests showed a similar bonding strength to that on smooth surfaces. In other words, the elliptic ditches did not significantly

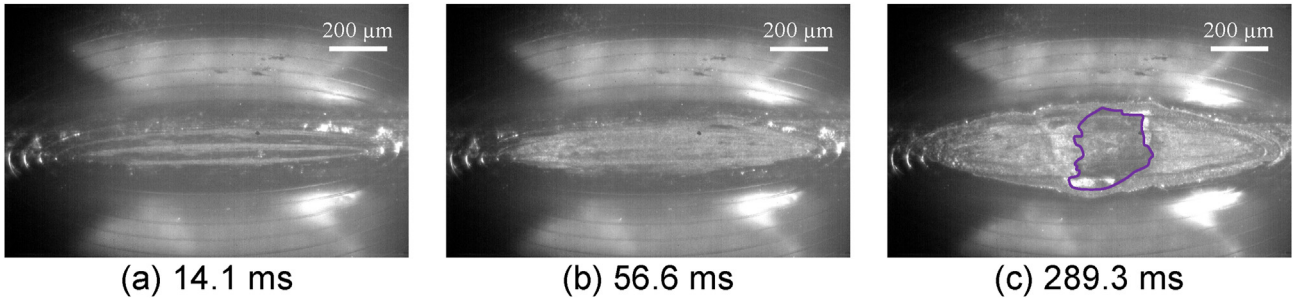

Fig. 12 – Wire bonding process with elliptic ditches of 10 μm width, 5 μm depth and 50 μm interval distance under 5 N, 0.35 A.

alter the bonding process and did not promote the oxide removal efficiency.

4. Conclusions

In this work, three textures including deposited strips, straight ditches and elliptic ditches, were tested for wire bonding. The results showed that the edges of deposited strips helped break the oxide scale. The oxide transportation occurred earlier and more oxides could be removed from inner peripheral region, compared to bonding on smooth surfaces. As for straight ditches, the cracking and milling were altered, and the efficiency of oxide removal was significantly promoted by chip generation. During the bonding process, aluminum and aluminum oxide were continuously cut from the wire, accumulated in the ditches, pressed and squeezed into long chips, and finally transported to the outside. Especially when the driving current exceeded 0.45 A, very long chips were generated. Accompanying with the growing of such chips, metal splashes were generated which further enhanced the oxide removal process. Compared to the bonding on smooth surfaces, the bonding strength on deposited strip and straight ditch textures was a few times higher, and the deviation of the strength became smaller. The bonding process window was significantly enlarged by these textures as well. The elliptic ditches had no significant influence on the bonding process.

Declaration of Competing Interest

The authors declare that they have no known competing financial interests or personal relationships that could have appeared to influence the work reported in this paper.

Acknowledgements

We gratefully acknowledge the support from Deutsche Forschungsgemeinschaft (German Research Foundation) with the project number 329797820. The publication of this article was funded by the Open Access Publishing Fund of Leibniz Universität Hannover.

REFERENCES

[1] Harman G. Wire bonding in microelectronics. McGraw-Hill Education; 2010.
[2] Osterwald F. Verbindungsbildung beim ultraschall-Drahtbonden: einflußder Schwingungs-parameter und Modellvorstellungen (Doctoral dissertation). Technical University of Berlin; 1999.
[3] Long Y, Twiefel J, Wallaschek J. A review on the mechanisms of ultrasonic wedge-wedge bonding. J Mater Process Technol 2017;245:241–58.
[4] Long Y, Dencker F, Isaak A, Hermsdorf J, Wurz M, Twiefel J. Self-cleaning mechanisms in ultrasonic bonding of Al wire. J Mater Process Technol 2018;258:58–66.
[5] Long Y, Dencker F, Isaak A, Li C, Schneider F, Hermsdorf J, et al. Revealing of ultrasonic wire bonding mechanisms via metal-glass bonding. Mater Sci Eng, B 2018;236:189–96.
[6] Unger A, Sextro W, Althoff S, Meyer T, Neumann K, Reinhart RF, et al. Data-driven modeling of the ultrasonic softening effect for robust copper wire bonding. In: 8th international conference on integrated power electronics systems; 2014. p. 1–11.
[7] Seppänen H, Kurppa R, Meriläinen A, Hæggström E. Real time contact resistance measurement to determine when microwelds start to form during ultrasonic wire bonding. Microelectron Eng 2013;104:114–9.
[8] Geissler U, Funck J, Schneider-Ramelow M, Engelmann HJ, Rooch I, Müller WH, et al. Interface formation in the US-wedge/wedge-bond process of AlSi1/CuNiAu contacts. J Electron Mater 2011;40(2):239–46.
[9] Khatibi G, Weiss B, Bernardi J, Schwarz S. Microstructural investigation of interfacial features in Al wire bonds. J Electron Mater 2012;41(12):3436–46.
[10] Long Y, He B, Cui W, Ji Y, Zhuang X, Twiefel J. Investigations on the mechanism of microweld changes during ultrasonic wire bonding by molecular dynamics simulation. Mater Des 2020;192:108718.
[11] Xu T, Walker T, Poncelet B, Fu J, Luechinger C. Consumable and process improvement for large copper wire bonding. In: International symposium on microelectronics; 2016. 000445-000449.
[12] Xu T, Walker T, Chen R, Fu J, Luechinger C. Bond tool life improvement for large copper wire bonding. In: 17th electronics packaging and technology conference; 2015. p. 1–5.
[13] Long Y, Twiefel J, Wallaschek J. Contact mechanics and friction processes in ultrasonic wire bonding-Basic theories and experimental investigations. J Sound Vib 2020;468:115021.